PUBLICATIONS OF THE ASTRONOMICAL SOCIETY OF THE PACIFIC, **118**: 860–865, 2006 June

The Pupil-swapping Coronagraph

O. GUYON

Subaru Telescope, National Astronomical Observatory of Japan, 650 North A'ohoku Place, Hilo, HI 96720; guyon@naoj.org

AND

M. SHAO

Jet Propulsion Laboratory, California Institute of Technology, 4800 Oak Grove Drive, Pasadena, CA 91109

Received 2006 January 26; accepted 2006 May 3; published 2006 June 14

ABSTRACT. A new coronagraph that performs destructive interference between copies of the telescope pupil in which "slices" have been swapped is studied in this paper. A fourth-order "pupil-swapping coronagraph" is particularly attractive for direct imaging of extrasolar terrestrial planets: it achieves 100% throughput at $1.4\lambda/d$ on a square pupil (72.5% at $1.77\lambda/d$ on a circular pupil), is compatible with a central obstruction and spiders, and delivers sharp images of off-axis sources. Direct detection of extrasolar terrestrial planets appears theoretically feasible on a 2 to 3 m visible-wavelength telescope in space.

1. INTRODUCTION

A coronagraph that is suitable for direct imaging of extrasolar terrestrial planets (ETPs) from space must simultaneously be able to tolerate small pointing errors (notably because the central star is partially resolved) and offer a small inner working angle (IWA; defined here as the minimum angular separation for which the coronagraph throughput reaches 50% of its maximum value).

Unfortunately, these two features are generally incompatible. Coronagraph designs with IWA $\approx \lambda/d$ are often too sensitive to stellar angular size to deliver sufficient contrast for direct imaging of ETPs. The achromatic interferometric coronagraph (Baudoz et al. 2000), the phase mask coronagraph (Roddier & Roddier 1997), and the four-quadrant phase mask coronagraph (Rouan et al. 2000) belong to this group. On the other hand, coronagraphs that can tolerate stellar angular size and small pointing errors usually have large IWAs ($3\lambda/d$ or more). These include the band-limited Lyot coronagraphs (Kuchner & Traub 2002), some designs of the apodized-pupil Lyot coronagraphs (Soummer et al. 2003), and the pupil apodization coronagraphs (Kasdin et al. 2003). Better compromises between IWAs and pointing sensitivity are offered by the phase-induced amplitude apodization coronagraph (Guyon 2003) and the visible nuller interferometer (Mennesson et al. 2003); both coronagraphs have IWAs of about $1.5\lambda/d$.

In this paper, a new coronagraph concept that offers a good compromise between throughput, IWA, and sensitivity to stellar angular size and pointing errors is proposed. The fourth-order pupil-swapping coronagraph is presented in § 2.1 and is shown to be closely related to the visible nuller interferometer. Its performance for direct imaging of ETPs is evaluated in § 3.2. Results are discussed in § 4.

2. FOURTH-ORDER PUPIL-SWAPPING CORONAGRAPH

2.1. Principle

The pupil-swapping coronagraph (PSC) principle is illustrated in Figure 1. A pupil-plane mask first subdivides the entrance pupil into four subpupils, A, B, C, and D. The pupil is first nulled against its "*X* swapped" copy. The resulting pupil is then nulled against its "*Y* swapped" copy. The resulting nulled pupil is also composed of four subpupils, A′, B′, C′, and D′. As illustrated in Figure 2, the PSC can be implemented with a small number of flat mirrors (four sets of two mirrors are assembled in "angle" mirrors to perform the *X* and *Y* swaps) and beam splitters.

Figure 1 shows that the complex amplitude across subpupils A′ and D′ are identical (equal to A − B − C + D) and opposite to the complex amplitudes across subpupils B′ and C′ (equal to −A + B + C − D). The complex amplitude across subpupil A′ is

$$A'(u, v) = (\sin \delta\pi x \sin \delta\pi y) e^{i\pi[(u+\delta/2)x/D+(v-\delta/2)y/D]}, \qquad (1)$$

where (u, v) are the pupil coordinates ($-\delta < u < 0$ and $0 < v < \delta$ for A′), (x, y) is the source position in units of λ/D, and δ is the subpupil size, as shown in Figure 1.

From equation (1), the "coronagraph throughput" (measured as the total flux in the nulled pupil) is

$$T(x, y) = M \sin^2 \delta\pi x \sin^2 \delta\pi y, \qquad (2)$$

where M is the throughput of the pupil mask used to produce the four subapertures. On a square pupil, $M = 1$ and $\delta = 0.5$: the throughput reaches 100% at $(x, y) = (1, 1)$ (angular sep-

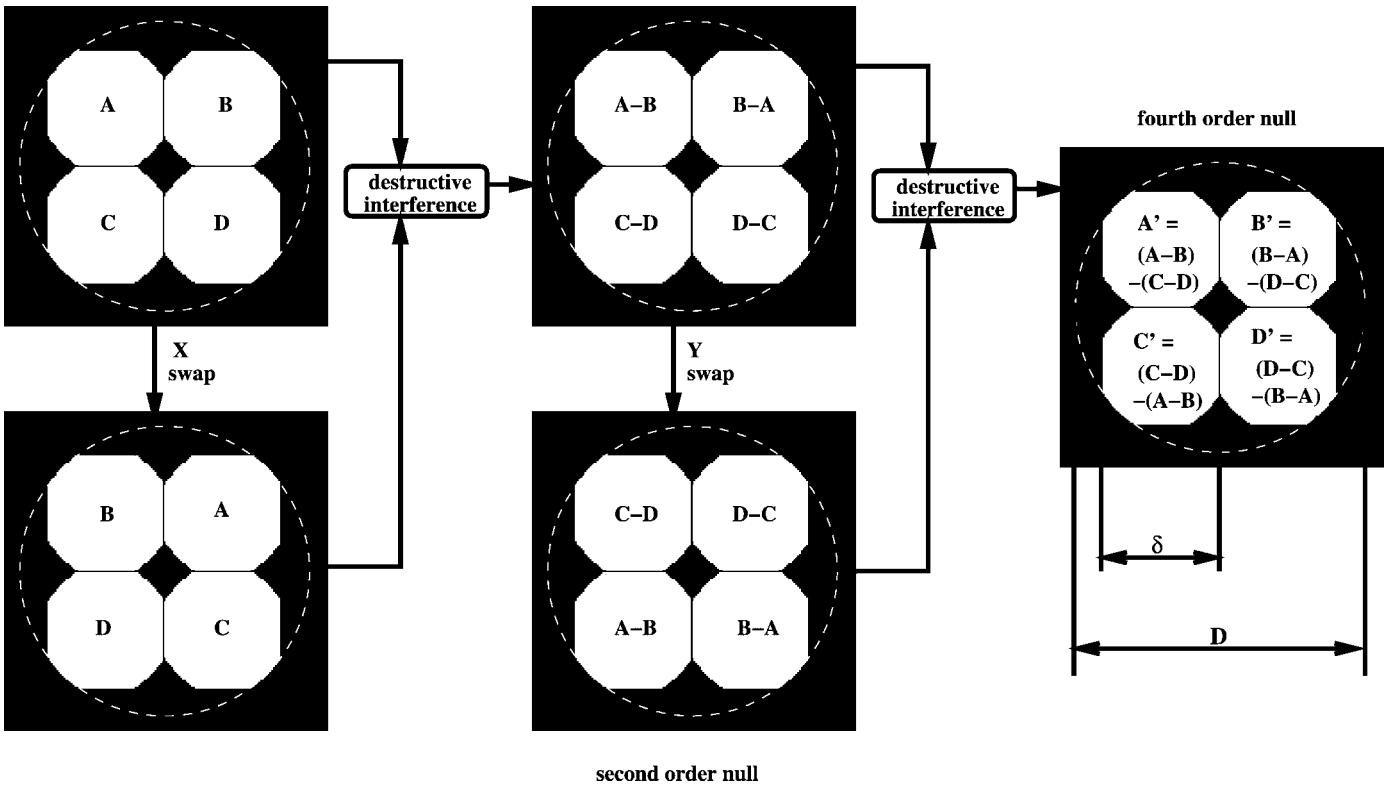

FIG. 1.—Principle of a fourth-order pupil-swapping coronagraph. The circular telescope pupil is masked (*top left*) to produce four subpupils (A to D). The two halves ($x > 0$ and $x < 0$) of the telescope pupil are swapped to produce the pupil shown at bottom left; this operation is referred to as an "*X* swap." Destructive interference between these two pupils yields the pupil shown in the top center column, which is combined with a "*Y* swapped" copy of itself (*bottom center*) to obtain the final nulled pupil (*right*).

aration $= 1.4\lambda/D$). On a circular pupil, the mask throughput is optimal for $\delta = 0.4$ ($M = 0.725$), and the first throughput maximum occurs at $(x, y) = (1.25, 1.25)$ (angular separation $= 1.77\lambda/D$). This last configuration is the one shown in Figure 1.

The fourth-order PSC's throughput is shown in Figure 3, where the first transmission peak at $1.77\lambda/D$ is clearly visible, followed by a low-throughput annulus at about $3\lambda/D$. In planet-searching mode, the poor sensitivity at $3\lambda/D$ is a disadvantage but can be mitigated by broadband observations. A better option would be to optically vary the "shear" parameter δ during observation or to implement the PSC on an elliptical pupil, for which δ would be different along the minor and major axes of the pupil.

2.2. Imaging with the Pupil-swapping Coronagraph

As demonstrated in § 2.1, the PSC's throughput is a two-dimensional periodic function of the source position. Figure 4 shows that the PSF shape varies rapidly across the field, and also periodically.

By writing equation (1) for each of the four subapertures, it is found that the pupil-plane complex amplitude is equal to A' convolved by a four-point kernel. The kernel's four points are on the corners of a δ-wide square, and their values are $+1$ for the top left and bottom right points, and -1 for the top right and bottom left points. The resulting pupil-plane complex amplitude is shown in Figure 5.

The PSC's point-spread function (PSF) for a source at position (x, y) on the sky can therefore be written as

$$\mathrm{PSF}(x, y, x', y') = 16\,\mathrm{PSF}_1(x, y, x', y') \times \sin^2 \delta\pi x \sin^2 \delta\pi y \sin^2 \delta\pi x' \sin^2 \delta\pi y', \quad (3)$$

where x' and y' are the coordinates in the focal-plane image and $\mathrm{PSF}_1(x, y, x', y')$ is the PSF delivered by a single fully illuminated subpupil. This result explains the PSF behavior identified in Figure 4: the PSC's PSF is equal to 4 times the PSF obtained by one subaperture, modulated by the $\sin^2 \delta\pi x \sin^2 \delta\pi y$ coronagraph throughput identified in § 2.1 and seen through a $4 \sin^2 \delta\pi x' \sin^2 \delta\pi y'$ "mask."

2.3. Comparison with a Visible Nuller Interferometer

In the visible nuller interferometer (Mennesson et al. 2003), the final nulled pupil is obtained through successive shears: one shear for a second-order null, and two orthogonal shears

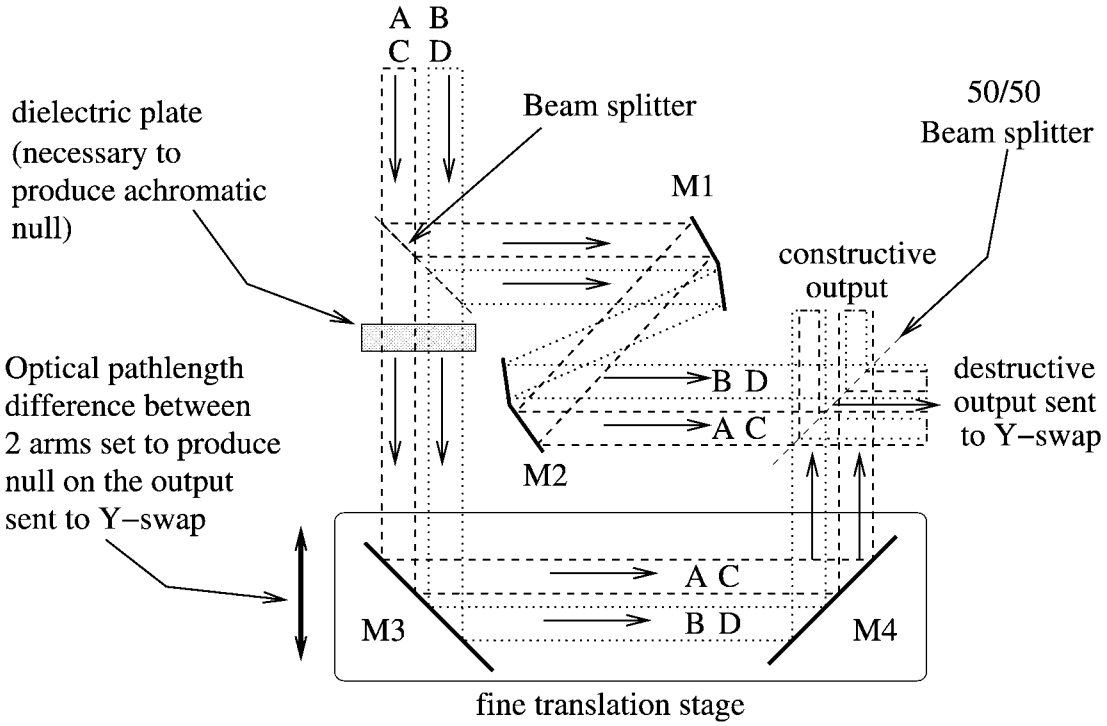

FIG. 2.—Schematic optical layout for the *X*-swapper and combiner. In this figure, the *X*-swap is performed by "angle" mirrors M1 and M2. The optical path length difference is fine-tuned to produce the null by translating mirrors M3 and M4. Without the M1 and M2 *X*-swapper, the interferometer shown in this figure would be a classical nulling combiner, and neither starlight nor planet light would be left in the destructive output.

for a fourth-order null. In the fourth-order configuration, referred to as the fourth-order visible nuller interferometer (VNI4) in this paper, the nulled pupil is identical to one of the four subpupils delivered by the PSC.

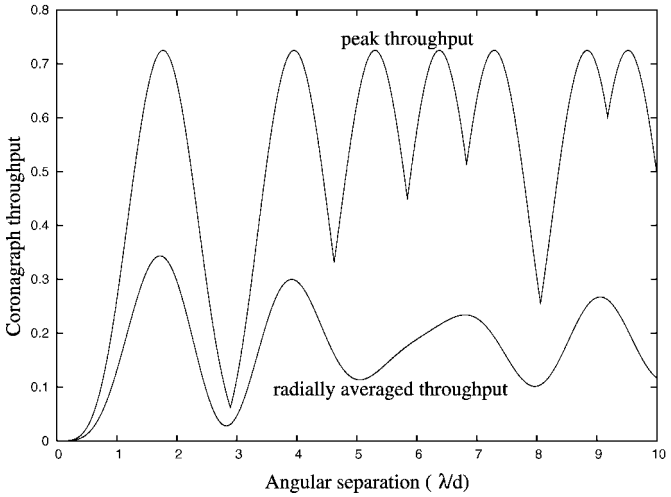

FIG. 3.—Peak and radially averaged throughput of the fourth-order PSC for a circular pupil. The peak throughput is reached when the position angle of the star-planet vector is favorable.

The PSC therefore offers, for the same pupil shear, roughly 4 times the throughput of the VNI4 (in fact slightly less, due to the constraint imposed by the nonoverlapping subpupils requirement in the exit pupil), with the same IWA.

It would seem that the PSC offers a gain in angular resolution: the PSF at the peak throughput is narrower than the PSF of a single subaperture. However, this effect is entirely due to the $\sin^2 \delta\pi x' \sin^2 \delta\pi y'$ multiplicative "masking" in equation (3) and is therefore purely a concentration of light in a smaller number of pixels, without increased angular resolution. Similarly, the PSC does not offer a better immunity to background contamination (zodiacal or exozodiacal light) than the VNI4: background light is also "masked" by the same $\sin^2 \delta\pi x' \sin^2 \delta\pi y'$ factor and is therefore also concentrated in the transmission peaks.

Thus, there is no fundamental performance increase between the PSC and the VNI4, other than an $\approx$4 times higher throughput. In a planet-imaging telescope, this gain is very significant, however, as it reduces exposure times by a factor of 4, which also relaxes wave-front stability requirements.

3. PERFORMANCE OF THE FOURTH-ORDER PSC

The main performance characteristics of the PSC are the following:

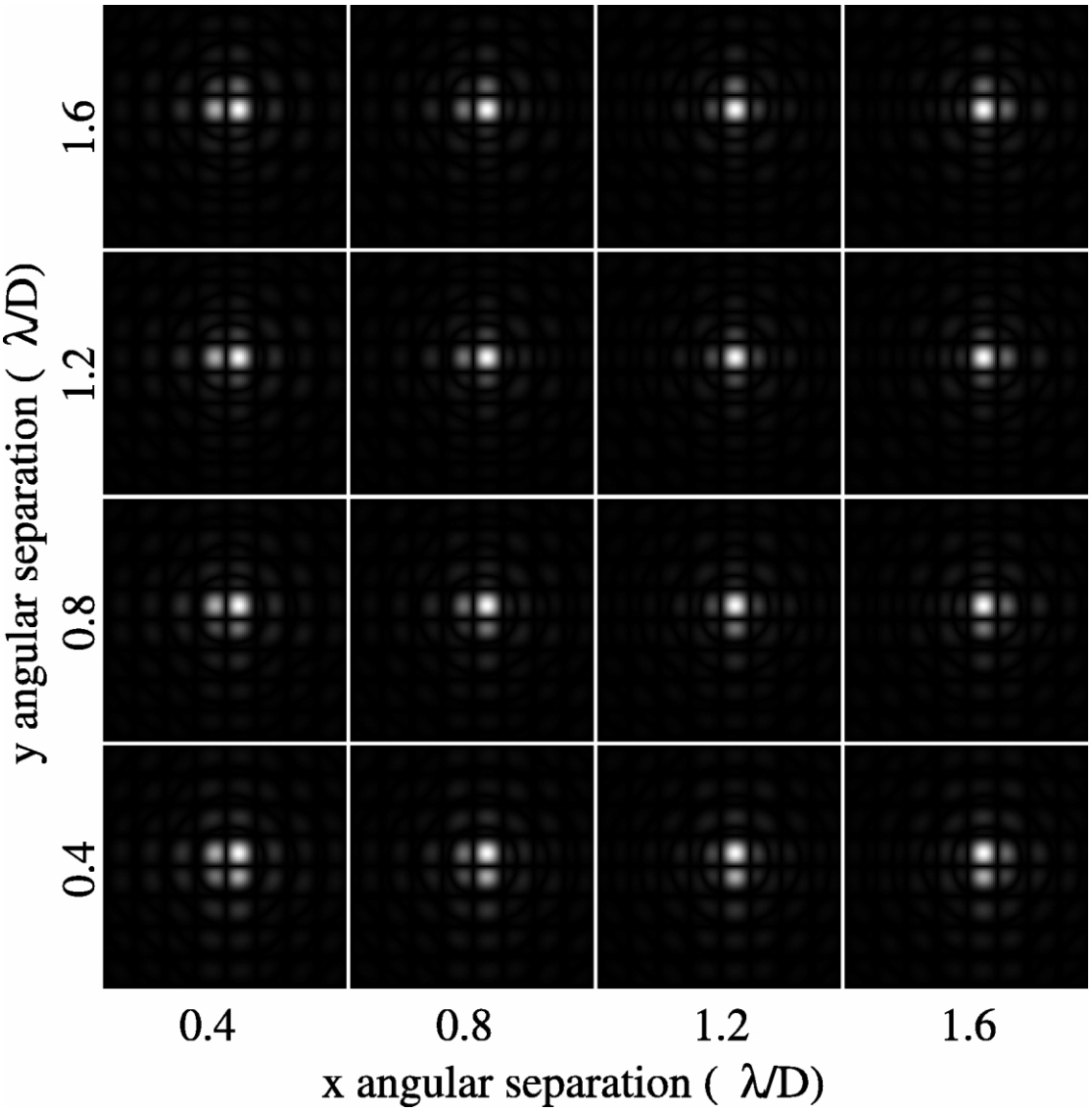

FIG. 4.—PSFs for several positions (x, y) of a point source on the sky. As described in the text, the image obtained by the PSC is equal to the image obtained by one of its four subapertures multiplied by a constant $4 \sin^2 \delta\pi x \sin^2 \delta\pi y$ and modulated by a $4 \sin^2 \delta\pi x' \sin^2 \delta\pi y'$ "mask," where x' and y' are the coordinates on the detector in λ/D.

IWA.—The coronagraph's throughput first reached 50% of the peak throughput at $1.12\lambda/d$ on a circular aperture.

Throughput.—The peak throughput is 72.5%, while the field-averaged throughput is 18%.

Angular resolution.—The "true" angular resolution of the PSC is $\approx 2\lambda/d$ (see § 2.3). About 4 times more background (zodiacal and exozodiacal light) is therefore mixed with the planet's light than in a noncoronagraphic classical telescope.

Sensitivity to stellar angular size.—The fourth-order null leaves some starlight on partially resolved stars.

3.1. Direct Imaging of Extrasolar Terrestrial Planets

Thanks to its small IWA and high peak throughput, the PSC may be suitable for a small telescope looking for Earth-type planets at $1\lambda/d$ to $4\lambda/d$. Keeping the planet-star angular separation below $\approx 5\lambda/d$ also ensures that starlight leaks due to the fourth-order null (the star is partially resolved) do not prevent planet detection. The suitability of the PSC for direct imaging of ETPs is illustrated in Figure 6: the planet signal is visible in this image, even before subtraction of the starlight residual. Exozodiacal light, not simulated in this work, could be a serious

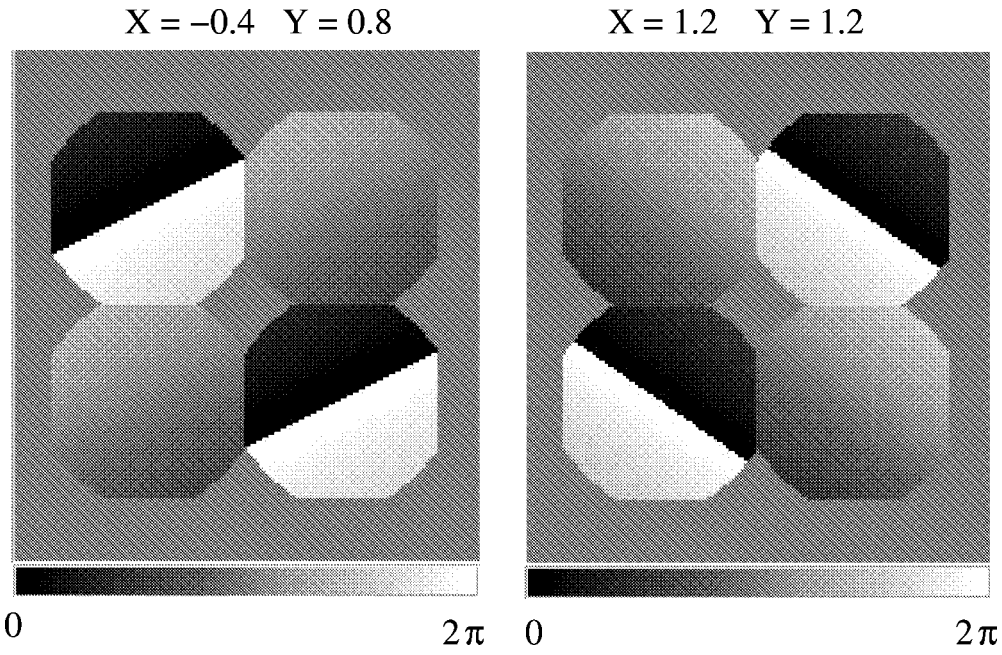

FIG. 5.—Phase in the output pupil plane (nulled output) for two source positions: $(-0.4\lambda/D, 0.8\lambda/D)$ and $(1.2\lambda/D, 1.2\lambda/D)$. The pupil-plane amplitude (not shown in this figure) is constant across the geometric pupil. The phase maps are identical in the top left and bottom right quadrants and are offset by π relative to the other two quadrants.

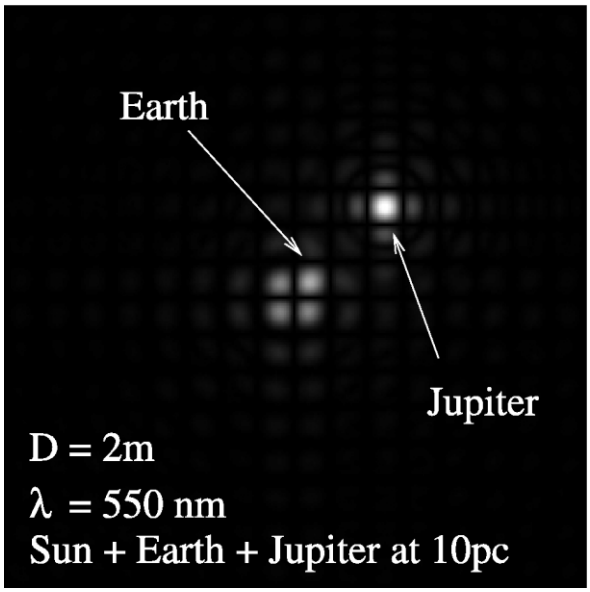

FIG. 6.—Simulated image of a Sun/Earth/Jupiter system at 10 pc with a 2 m visible-wavelength telescope. Both planets were assumed to be at maximum elongation. Earth is at 0.″1 separation, 2×10^{-10} contrast. Jupiter is at 0.″5 separation, 9.2×10^{-10} contrast. The angular diameter of the Sun at 10 pc (1 mas) is responsible for the four bright diffraction peaks in the center of the image. The Earth is seen on top of one of these four peaks, making it approximately twice as bright as the others. No zodiacal light, exozodiacal light, or photon noise was included in this simulation. In this example, both planets happen to fall close to throughput maxima.

problem, however, as exozodiacal clouds are expected to be much brighter than an ETP and may not be perfectly symmetric. An asymmetric exozodiacal cloud would produce an excess of light on one side of the null, just like the planet signature in Figure 6. Direct detection of ETPs with a PSC on a small telescope is therefore challenging but may be possible around a handful of stars.

3.2. Direct Imaging of Jupiter-Type Planets

Jupiter-type planets are significantly easier to detect: Jupiter is 5 times farther out and ≈5 to 10 times brighter than Earth. At 5 AU, exozodiacal light is weak and does not pose a serious problem. The larger planet-star separation, combined with the brighter planet, allows the use of a smaller telescope and/or observation of a more distant sample of stars. Figure 6 illustrates how the PSC on a 2 m visible telescope could in theory "easily" pick up Jupiters at 10 pc.

4. DISCUSSION

The PSC's ability to reach high peak throughput very close to the star is unique: low-IWA coronagraphs are usually unable to maintain high contrast on partially resolved stars. The PSC appears to be especially valuable when the planet's position is already known, and the instrument/telescope can be properly oriented to maximize throughput at the planet's position. Acquisition of a planet's spectrum, which requires significantly

longer integration times than for planet detection, can then fully benefit from the high peak throughput.

The fourth-order PSC concept illustrated in Figure 1 could be extended to deeper nulls. For example, an eighth-order null could be obtained by cascading two fourth-order PSCs: the second PSC would operate within each of the four subapertures in the output of the first PSC. The resulting nulled pupil would be composed of 16 subapertures. However, in this concept, the price to pay for a deeper null may be too high: low average throughput ($1/16 = 6.25\%$ for a square pupil and the eighth-order PSC described above) and low angular resolution ($4\lambda/d$ in the same example). The fourth-order PSC presented in this work seems to be a good compromise between throughput, angular resolution, and null depth. Its small IWA ($1.12\lambda/d$ at the 50% throughput level) and high peak throughput (72.5%) on a circular pupil make it a competitive coronagraph.

The PSC can also accept a central obstruction and four spiders without performance loss and could therefore be implemented on existing large, ground-based telescopes that are equipped with adaptive optics. Some telescopes have offset spiders, or three spiders rather than four. The corresponding subpupil mask would have a lower throughput, as a spider that crosses only one of the four subpupils A to D in Figure 1 needs to be masked in each of the subpupils to maintain the destructive interference. In the most unfavorable geometries, this could multiply by 4 the fraction of the pupil area lost due to spiders.

REFERENCES

Baudoz, P., Rabbia, Y., & Gay, J. 2000, A&AS, 141, 319
Guyon, O. 2003, A&A, 404, 379
Kasdin, N. J., Vanderbei, R. J., Spergel, D. N., & Littman, M. G. 2003, ApJ, 582, 1147
Kuchner, M. J., & Traub, W. A. 2002, ApJ, 570, 900
Mennesson, B. P., Shao, M., Levine, B. M., Wallace, J. K., Liu, D. T., Serabyn, E., Unwin, S. C., & Beichman, C. A. 2003, Proc. SPIE, 4860, 32
Roddier, F., & Roddier, C. 1997, PASP, 109, 815
Rouan, D., Riaud, P., Boccaletti, A., Clénet, Y., & Labeyrie, A. 2000, PASP, 112, 1479
Soummer, R., Aime, C., & Falloon, P. E. 2003, A&A, 397, 1161